Energy Storage Materials 33 (2020) 88–94

Contents lists available at ScienceDirect

Energy Storage Materials

journal homepage: www.elsevier.com/locate/ensm

Probing the electrochemical evolutions of Na–CO2 nanobatteries on Pt@NCNT cathodes using in-situ environmental TEM

Yuanmin Zhu [a,b,1], Shihui Feng [a,1], Peng Zhang [a], Mohan Guo [c], Qi Wang [a], Duojie Wu [a], Lei Zhang [d], Hui Li [a], Haijiang Wang [a], Lang Chen [c], Xueliang Sun [d], Meng Gu [a,*]

[a] Department of Materials Science and Engineering, Southern University of Science and Technology, Shenzhen, 518055, China
[b] SUSTech Academy for Advanced Interdisciplinary Studies, Southern University of Science and Technology, Shenzhen, 518055, China
[c] Department of Physics, Southern University of Science and Technology, Shenzhen, 518055, China
[d] Department of Mechanical and Materials Engineering, University of Western Ontario, London, Ontario, N6A 5B9, Canada

ARTICLE INFO

Keywords:
Na-CO_2 nanobattery
In situ ETEM
Single atom catalyst
Electrochemical evolution
Structure evolution

ABSTRACT

Na–CO_2 batteries possess many virtues including low cost, abundant sodium-containing resources, and environment-friendly nature. Understanding the electrochemical reaction processes is fundamental for battery design and performance enhancement of Na–CO_2 batteries. Using *in-situ* environmental transmission electron microscopy in CO_2 gas, we directly probed the morphology evolution and phase transformations of the charge and discharge products with single Pt atom and nitride doped carbon nanotube (Pt@NCNT) cathode in a Na–CO_2 nanobattery. The discharge reaction produces Na_2CO_3 and carbon, which subsequently decomposed into Na ions and CO_2 during charge. The discharge rate was boosted with the help of the single-atom Pt catalyst. Our work provides a fundamental insight into the governing principles on Na–CO_2 battery design for better energy storage devices.

1. Introduction

To fulfill the ever-increasing energy demand and alleviate the greenhouse effect, the development of green energy storage has enticed many scientists to invent more powerful batteries going beyond regular Li-ion batteries [1,2]. The high theoretical energy density of alkali metal (Li, Na, K)-air battery system [3,4] makes them attractive options for next-generation batteries. However, parasitic products, reversibility issues, and lack of efficient catalysts in Li- and Na–O_2 batteries limit their cycle life [5]. Further, the impurities of oxygen also lead to the formation of irreversible carbonates and hydroxide in Li- and Na–O_2 batteries [6–10].

Archer et al. created metal-CO_2 batteries and increased its efficiency to be higher than Li–O_2 battery [11]. Besides, the consumption of carbon dioxide in metal-CO_2 batteries also helps alleviate the crisis of global warming. Recently, numerous works focus on the development of electrolyte and electrode materials to increase cycling life and theoretical energy density [12–16]. Using O_2 and CO_2 as air cathodes results in different reaction steps and discharge products [10,17]. Some researchers reported that a mixed atmosphere of oxygen and carbon dioxide can enhance the performance of metal-air batteries [5,11,18]. But only a few works pay attention to the understanding of electrochemical reactions between metals and CO_2 at nanoscale and exploration of underlying fundamental reaction mechanisms [19–22]. In-situ characterization techniques are important to investigate its electrochemical processes, which allows us to observe the reaction process directly and get to details of reaction products [23–25].

Here, we used in-situ environmental transmission electron microscope (ETEM) to monitor Na–CO_2 nanobatteries to unveil the electrochemical reaction products and probe the reversibility of the reactions. To promote the discharge/charge process, the single atom Pt doped NCNT was used as the cathode. The Na–CO_2 nanobattery was constructed by using single platinum atom on nitrogen-doped carbon nanotube (Pt@NCNT) as air cathode, and metal sodium (Na) as ion source in CO_2 atmosphere. Morphology evolution during the discharge/charge process was recorded and reaction products were also identified using selected area electron diffractions (SAED). To minimize the damage of the electron beam, all experiment was conducted at an accelerating voltage of 80 kV in the ETEM. Furthermore, the usage of single platinum atom catalysts on NCNT as cathode support material in present work is designed to promote the cycling performance of Na–CO_2 batteries.

* Corresponding author.
E-mail address: gum@sustech.edu.cn (M. Gu).
[1] These authors contributed equally to this work.

https://doi.org/10.1016/j.ensm.2020.07.019
Received 2 April 2020; Received in revised form 2 July 2020; Accepted 13 July 2020
Available online 8 August 2020

2. Result and discussion

The low and high magnified morphologies of Pt@NCNT in Fig. 1a and b confirmed the presence of high density of single Pt atoms as highlighted in red circles in Fig. 1b. Elements distribution of pristine Pt@NCNT were shown in Fig. S1. Fig. 1c illustrates a schematic setup of the Na–CO_2 nanobattery. The Na–CO_2 nanobattery was constructed by a metal sodium anode glued on a tungsten tip, a Na_2O thin layer grown on Na metal surface as solid electrolyte, and Pt@NCNT as cathode under 1 mbar CO_2 atmosphere, as depicted in Fig. 1c. The incorporation of two electrodes was conducted in an STM holder. Detailed information about assembling procedures of this Na–CO_2 nanobattery was described in the method section.

Fig. 2 shows the morphology evolutions during the discharge/charge process, which can also be viewed in Movie S1. At the beginning of discharge, sodium ions first intercalate into Pt@NCNT and the reaction front is labeled by the red arrows in Fig. 2a. It indicates the NCNT can serve as a sodium ion conductor as well as a good electron conductor. Additionally, sodium ion transportation is not only observed in the inner part of NCNT but also on its surface (yellow arrow in Fig. 2a), which causes nearly 10 nm increasing to a lateral thickness of NCNT. After about 40 s, intercalation rates of Na ions into NCNT decreased and a nanoscale ball-shaped discharge product nucleated and grew (orange circle in Fig. 2a). Interestingly, the ball-shaped product was not grown at the triple interface of NCNT, CO_2, and Na, but on the surface of Pt@NCNT. This phenomenon confirms that the discharge reactions between Na and CO_2 cathode can take place on the surface due to the highly conductive Na^+ ion transport of Pt@NCNT. Fig. 2b shows the charge process of the nanobattery with a reversed voltage (+1 V) and the discharge product ball on the surface shrank gradually until entirely disappeared. Furthermore, Fig. 2c and d shows the second discharge/charge circle of the same Pt@NCNT-Na nanobattery. Similar to the first cycle, the discharge product emerged on the surface of NCNT and decomposed during the charge process. It is noted that the discharge/charge process can repeat several times, confirming the repeatability of such Na–CO_2 nanobattery using such designed air cathode (Movie S2-S3 and Figs. S2–3). The growth rate of the ball-shaped product was calculated and plotted in Fig. 2e. The blue, red and green lines represent the growth curves of discharge products in the Pt@NCNTs for discharge reaction product 1#, 2# and 3#, respectively (observed in Fig. 2 and Movie S1). The magenta line shows the growth rate of the discharge product (4#) in Fig. S2 and Movie S2.

Supplementary data related to this article can be found at https://doi.org/10.1016/j.ensm.2020.07.019.

In comparison, in-situ experiments of the Na–CO_2 nanobattery using pure NCNT without Pt catalysts were conducted and the morphology evolutions were captured in Figs. S4–S6 and Movie S4. The pure NCNT air cathodes exhibited similar product formation and evolution with the Pt@NCNT air cathode. However, the discharge and charge rate were much lower. The olive, dark blue and purple line refers to the discharge growth curve of the product on the pure NCNT in Fig. 2e, about one order slower than that of the NCNT with single-atom Pt catalyst. The calculated growth rate of reaction product balls is linear with time, revealing a diffusion-controlled growth mechanism of the discharge products in this Na–CO_2 nanobattery [22]. The real discharge growth rate is $\sim 2.5 \times 10^4$ nm^3/s for Pt@NCNT cathodes, about one order magnitude higher than that of the pure NCNT ($\sim 3.4 \times 10^3$ nm^3/s), indicating that the Pt single-atom catalyst can greatly boost the reaction rate of this electrochemical reactions in the Na–CO_2 nanobatteries.

Supplementary data related to this article can be found at https://doi.org/10.1016/j.ensm.2020.07.019.

Crystalline structure of the reaction product during discharge and charge in Na–CO_2 nanobattery was *in-situ* recorded using selected area electron diffraction patterns (SAEDPs) (Fig. 3a and b). The selected sample areas for SAED during discharge/charge were shown in Fig. S7. Diffraction rings of NCNT (004) plane and Na_2O (200) plane were observed in SAEDP of the pristine NCNT before discharge (left of Fig. 3a). The SAEDPs of the NCNT and product balls during discharge for 100s shows a series of diffraction rings indexed as the NCNT (004) and Na_2CO_3(100), (200) and (301) crystal planes, indicating the formation of Na_2CO_3 during discharge process (Fig. 3a, right). During charge, the product began to shrink and corresponding SAEDPs evolved to be body center cubic sodium metal phase (Na (200) and (−110) spots), which indicates the decomposition of Na_2CO_3 products to metal Na in Fig. 3b. The weak rings of reaction product Na_2CO_3 slightly remain in the SAEDPs, showing the residual Na_2CO_3 present in NCNT. Fig. 3c shows the corresponding profiles of integral intensity of the SAEDPs in Fig. 2a&b, which directly compares the reaction products in different stages of the electrochemical reaction. Therefore, during the discharge evolution, our SAEDPs proved that the discharge reaction to form Na_2CO_3 product at the surface of Pt@NCNT as: $4Na^+ + 4e^- + 3CO_2 \rightarrow 2Na_2CO_3 + C$. The charge process consists of the decomposition of the Na_2CO_3 ball into Na at the surface and de-intercalation of Na ion in NCNT, which corresponds to the reactions as reported in the Na–CO_2 batteries: $2Na_2CO_3 + C \rightarrow 4Na + 3CO_2$ [26].

To further confirm the result of SAED analysis. The structure and composition identity of the discharge product on the surface of the NCNT is tracked by electron energy loss spectroscopy (EELS) and energy dispersive spectroscopy (EDS). Detailed experiment conditions can be found in the experimental section. Through the fine structure of the EELS,

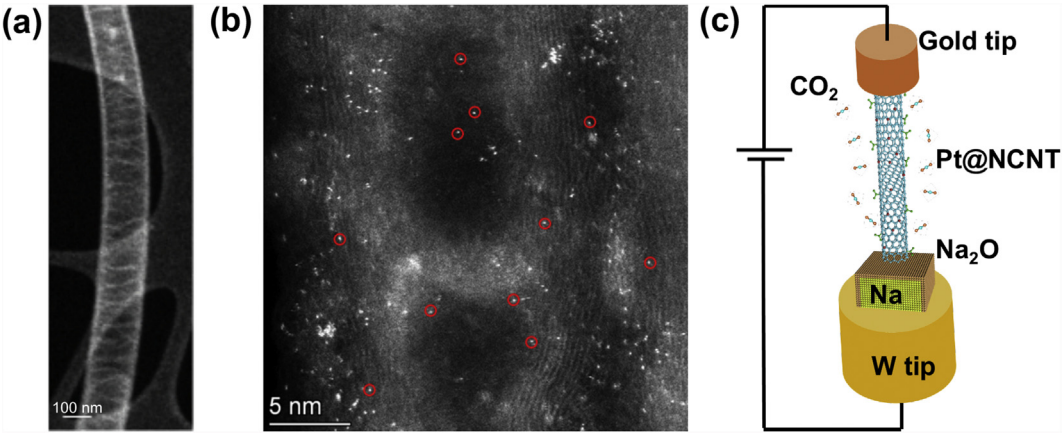

Fig. 1. STEM-HAADF images of Pt@NCNT at low magnification (a) and high magnification (b). (c) schematic figure of constructed Na–CO_2 nanobattery in ETEM. Red circle in Fig. 1b shows the presence of single Pt atoms. (For interpretation of the references to colour in this figure legend, the reader is referred to the Web version of this article.)

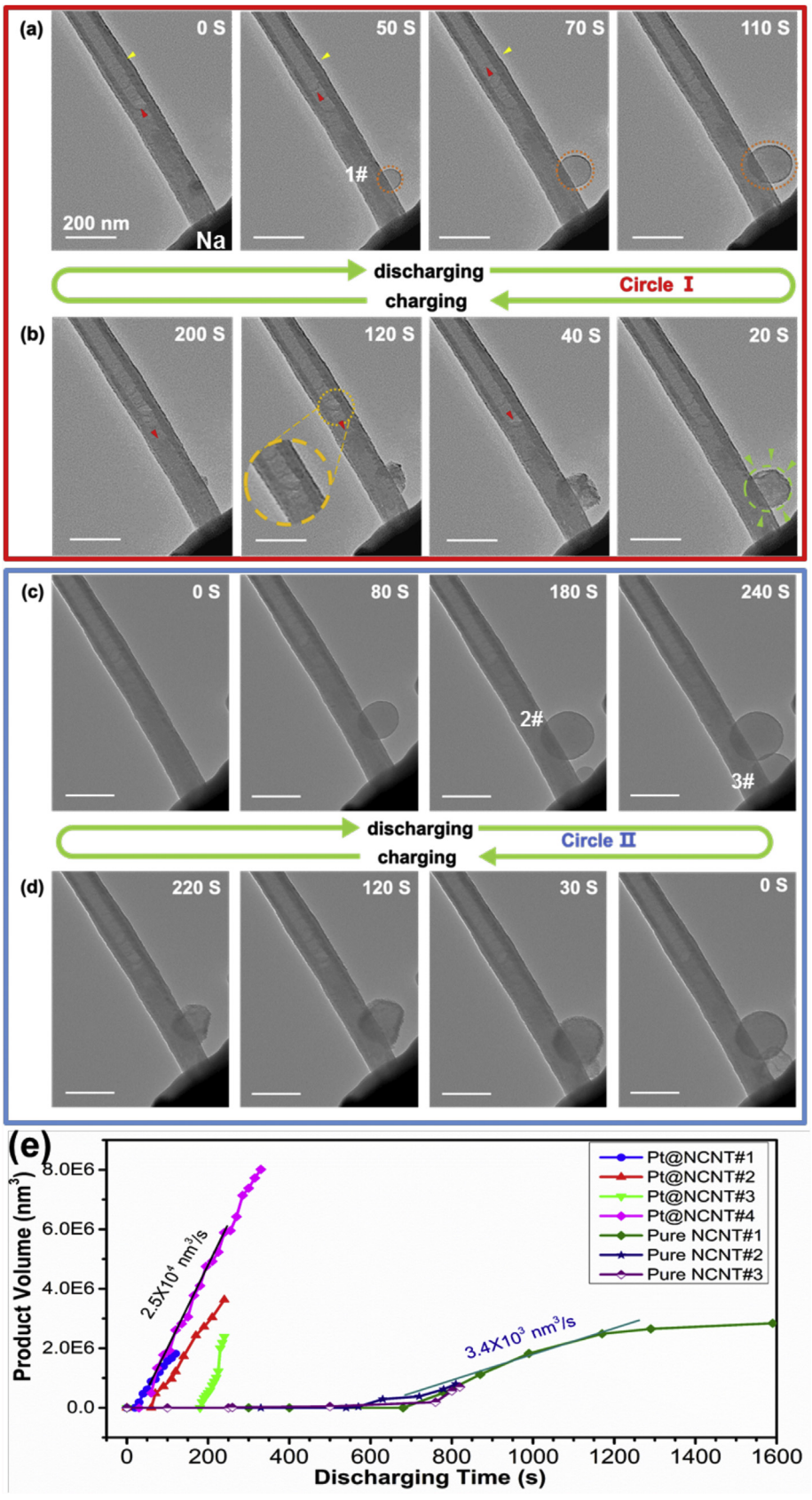

Fig. 2. Morphology evolution of a single platinum atom doped NCNT (Pt@NCNT) during discharge (a) and charge (b) electrochemical process in Na–CO_2 nanobattery (circle I); (c, d) discharge and charge evolution during circle II. All scale bars represent 200 nm. White mark 1#, 2#, 3# refers to the numbers of reaction products. (e) Growth rate of discharge products (ball) during discharge.

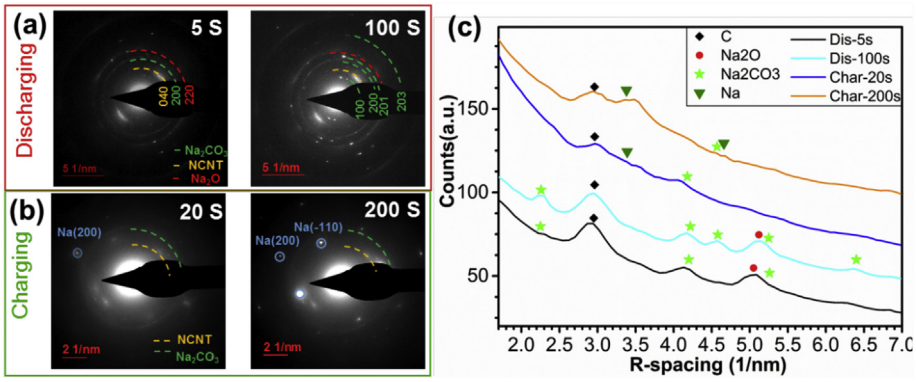

Fig. 3. Reaction and structural analysis of the Na–CO_2 nanobattery. Selecting area electron diffraction pattern (SAEDP) of the reaction products at the surface of NCNT during the cycling, (a) Discharge process and (b) Charge process. (c) Profiles of the integral intensity of the SAED patterns in (a) and (b) over time.

we further verify the composition and valence state changes in the pristine and discharged NCNT including the reaction balls. The spectrum of pristine NCNT (black spectrum in Fig. 4a) shows a core-loss peak of carbon *K* edge at 284.4 eV. The N *K* edge is also characterized by a major peak at 406.8 eV, while a small oxygen *K* edge is also observed at 537.2 eV, which is corresponding to a little hydroxide radical at the surface of NCNT. It confirms the purity NCNT before discharge. After discharge, the EELS (Redline) in Fig. 4b shows the presence of core-loss peaks ascribed to the Na *K* edge at 1078 eV, carbon *K* edge and oxygen *K* edge. The pronounced O *K* edge at 538.5 eV after discharge is consistent with the formation of Na_2CO_3. C *K* edge also observed in EELS after discharge reaction by a major peak at 286.0 eV with a chemical shift of about +1.6 eV towards higher energy compared to the original C *K* edge in CNT. The intensity of the second peak in carbon *K* edge also increased significantly. Considering the high intensity of O *K* edge, Na *K* edge, and the high valence state of carbon, we deduce the formation of Na_2CO_3 as the discharge products. Our EELS analysis is in good agreement with SAEDPs results as shown in Fig. 3b. Fig. 4b presents the EDS mapping of NCNT after discharge-charge processes and residual discharge products were observed on the surface of NCNT, which again proves that the reaction products contain Na, C and O elements.

To confirm the rechargeability and stability of our nanobattery, more discharge/charge cycles were conducted. Fig. 5 shows periodical voltage variations against a Pt@NCNT cathode and corresponding dynamic movies can be found in Movies S5-6. By controlling the displacement of tungsten tips, we can separate and rebuild the connection between the sodium anode and Pt@NCNT cathode. Fig. 5a–b is discharge-charge circles I and II of this Na–Pt@NCNT electrode with an obtuse angle, the reaction products emerge during discharge and decomposed at charge process. Fig. 5c–d shows the subsequent circles III and IV of the same Na–Pt@NCNT with intentionally rebuilt connection of Na source and Pt@NCNT, where the electrochemical morphology evolutions are the same compared to the previous observations in Fig. 5a and b. It demonstrated that our Na–CO_2 nanobattery can circling stably at different connection conditions of the Na–Pt@NCNT.

Supplementary video related to this article can be found at https://doi.org/10.1016/j.ensm.2020.07.019

Based on *in-situ* ETEM experiments, a schematic drawing in Fig. 6 can illustrate the reaction mechanism during the discharge/charge electrochemical process. The simplified nanobattery consists of metal Na, Na_2O solid electrolyte, a single NCNT loaded with platinum atoms and a CO_2 atmosphere. When applying a negative voltage to Pt@NCNT side, the discharge was initiated through the intercalation of Na^+ ions into the NCNT and also transportation of Na^+ on the surface. After discharge for a while, the intercalation rate slows down, and then the Na^+ reacts with CO_2, leading to the formation of Na_2CO_3 at the surface of the NCNT. The Na_2CO_3 ball emerged on the surface of Pt@NCNT, in which the single platinum atom catalyst may play important roles. Not only that, some works confirmed the doping of the single atom catalyst could accelerate the electrochemical process and improve the stabilities of Na-Air batteries [23,27].

During discharge, Na^+ firstly comes across the layer of Na_2O electrolyte, at the same time, electrons were transported in opposite direction in outside circuits. The Na^+ and electrons react with CO_2 molecules following routes as follows [26]:

$$\text{Anode: } Na \rightarrow Na^+ + e^- \quad (1)$$

$$\text{Cathode: } 4Na^+ + 4e^- + 3CO_2 \rightarrow 2Na_2CO_3 + C \quad (2)$$

During charge, the reaction product is likely decomposed to Na metal with the consumption of carbon on NCNT, the charge reaction takes place as:

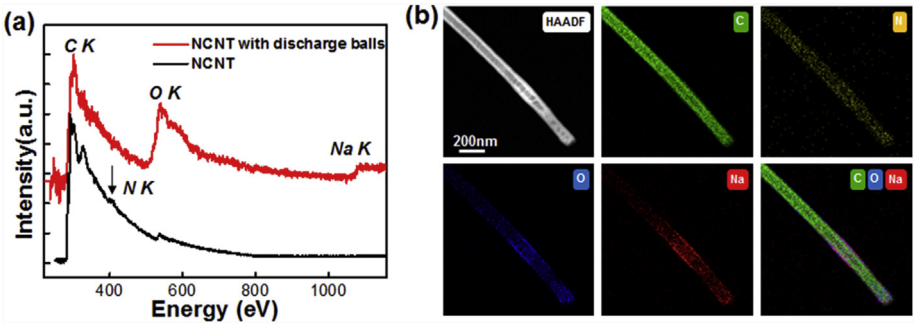

Fig. 4. Chemical analysis of discharge products on NCNT. (a) electron energy loss spectrum of pristine NCNT (black) and discharge product area including the reaction balls (red). (b) EDS mapping of NCNT after discharge/charge processes. (For interpretation of the references to colour in this figure legend, the reader is referred to the Web version of this article.)

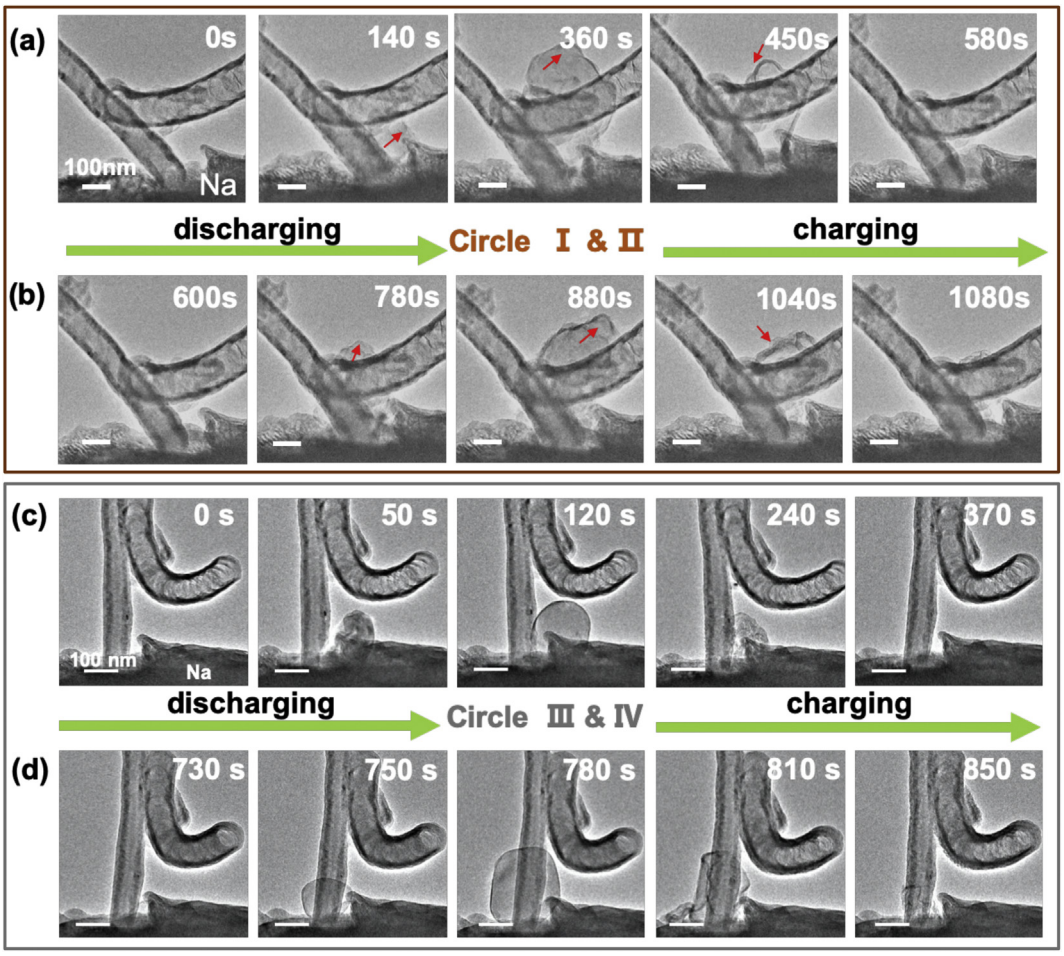

Fig. 5. Repeatable morphology evolution of discharge/charge process with different contact angle between sodium anode and Pt@NCNT cathode. (a–b) the discharge-charge circle I (a) & II (b) under contact angle alpha (larger than 90°). (c–d) the discharge-charge circle III (c) & IV (d) under contact angle beta (right-angle). Scale bar, 200 nm.

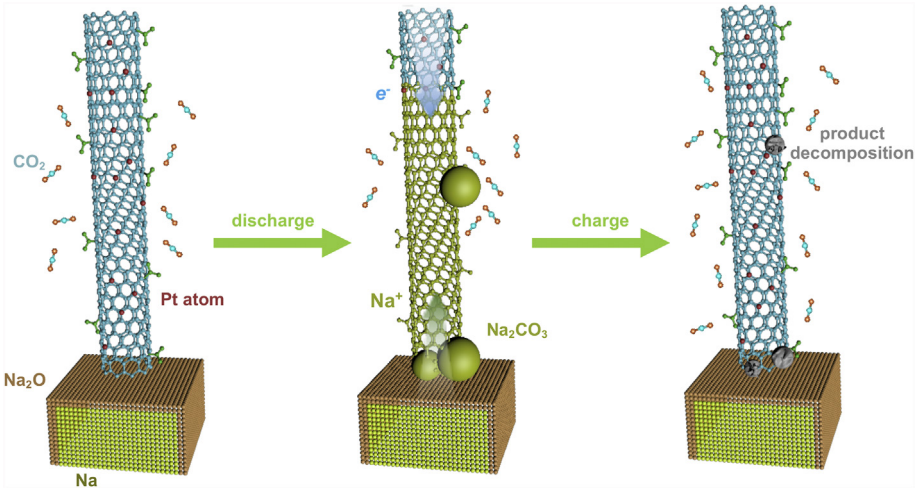

Fig. 6. Schematics for the discharge/charge electrochemical processes in the Na–CO2 nanobattery.

$2Na_2CO_3 + C \rightarrow 4Na + 3CO_2$

Please note that it is difficult to differentiate the carbon product from reactions with NCNT. Nevertheless, the *in-situ* ETEM provides evidence and a plausible explanation of the above reaction mechanism.

To validate the electrochemical processes, the real button cells using the same single Pt@NCNTs as air cathodes were assembled and the measured results were shown in Fig. S8. The assembled Na–CO_2 cell with Pt@NCNT cathode exhibits a typical discharge plateau around 1.5 V (Fig. S8a), indicating the formation of Na_2CO_3 according with in-situ TEM data and previous reports. CV results present the significantly enhanced reduced and evolved current density of CO_2 (Fig. S8b) by the

modification of monatomic Pt, demonstrating the critical role of monatomic Pt in the electrochemical reaction.

To demonstrate the effect of the CO_2 atmosphere, a controlled experiment was conducted in a vacuum without CO_2 gases in Fig. S9. No ball-shaped products were observed during the discharge process. Therefore, the reactions observed in this paper are real Na metal-CO_2 battery reactions.

Furthermore, to investigate the possible functional difference between Pt particle catalyst and single atom catalyst on the NCNT, NCNT decorated with Pt particles catalyst were used in our in-situ TEM observation in CO_2 atmosphere. Fig. S10 shows the morphology evolution of Na–CO_2 nanobattery using NCNT with Pt particles as the air cathode. Red circles in Fig. S10a label the presence of Pt particles on NCNT and red arrows in Figs. S10b–h indicates the growth/decomposition orientations of reaction products. These reaction products are similar with Pt single atom catalyst on NCNT in terms of ball-shaped products, morphology evolution, and reaction rates. However, Pt single atom on NCNT uses less precious Pt, largely reducing the consumption of platinum.

In addition, beam effects have to be considered in TEM observations of energy storage materials. The knock-on damage caused by high-voltage electrons may lead to decomposition of products or arrest of product development if high doses of electrons are used. In order to avoid the beam effect, we decrease electron beam voltage to 80 kV and a low dose rate (<0.5 e/Å^{2}s) during in-situ experiments. In these conditions, we observe no significant contribution of electron beam on our battery reactions. In contrast, we also intentionally acquire in-situ movies with high magnifications and high dose rate (~2.0 e/Å^{2}s) of electron beam in Movie S7. Many small ball-shaped products formed on the Pt@NCNT, however, these ball-shaped products did not grow as large as other low-dose experiments. In addition, high electron dosage led to faster decomposition of products (Na_2CO_3) as observed in the in-situ nanobattery. In conclusion, electron beam effects have to be controlled in the in-situ TEM experiments.

Supplementary data related to this article can be found at https://doi.org/10.1016/j.ensm.2020.07.019.

3. Conclusions

In conclusion, repeatable discharge/charge cycles of Na–CO_2 nanobattery on the Pt@NCNT were directly imaged using *in-situ* ETEM. The fundamental reaction mechanism was revealed using SAEDPs and EELS analysis. During discharge, Na_2CO_3 reaction balls formed on the surface of Pt@NCNT. During charge, Na_2CO_3 products decomposed into Na metal and CO_2. We also showed the single Pt single atom doped NCNT are an efficient catalyst for Na–CO_2 batteries. The promising cycling performance of a real Na–CO_2 battery using Pt@NCNT was also demonstrated. Our results provide an in-depth understanding of the working mechanism of Na–CO_2 battery, inspiring us to come up with novel designs of environmentally beneficial Na–CO_2 battery and catalysts.

Experimental procedures

Detailed experimental section is provided in the Supplemental information.

CRediT authorship contribution statement

Yuanmin Zhu: Methodology, Investigation, Writing - original draft, Formal analysis, Data curation. **Shihui Feng:** Investigation, Writing - original draft, Formal analysis, Data curation. **Peng Zhang:** Data curation. **Mohan Guo:** Visualization. **Qi Wang:** Visualization. **Duojie Wu:** Data curation. **Lei Zhang:** Resources. **Hui Li:** Resources. **Haijiang Wang:** Resources. **Lang Chen:** Resources, Writing - review & editing. **Xueliang Sun:** Resources, Writing - review & editing. **Meng Gu:** Supervision, Conceptualization, Writing - review & editing, Funding acquisition.

Declaration of competing interest

The authors declare that they have no known competing financial interests or personal relationships that could have appeared to influence the work reported in this paper.

Acknowledgements

The work is supported by National Natural Science Foundation of China (No.21802065), Guangdong Innovative and Entrepreneurial Research Team Program (2016ZT06N500), Shenzhen fundamental research project (JCYJ20190809181601639), Shenzhen DRC project [2018]1433, Shenzhen Clean Energy Research Institute (No. CERI-KY-2019-003). This work used the resources of the Pico Center from SUSTech Core Research Facilities that receives support from the Presidential Fund and Development and Reform Commission of Shenzhen Municipality.

Appendix A. Supplementary data

Supplementary data to this article can be found online at https://doi.org/10.1016/j.ensm.2020.07.019.

References

[1] M. Park, J. Ryu, W. Wang, J. Cho, Material design and engineering of next-generation flow-battery technologies, Nat. Rev. Mater. 2 (2017) 16080, https://doi.org/10.1038/natrevmats.2016.80.
[2] X. Mu, H. Pan, P. He, H. Zhou, Li–CO2 and Na–CO2 batteries: toward greener and sustainable electrical energy storage, Adv. Mater. 1903790 (2019) 1–22, https://doi.org/10.1002/adma.201903790.
[3] G. Girishkumar, B. McCloskey, A.C. Luntz, S. Swanson, W. Wilcke, Lithium−Air battery: promise and challenges, J. Phys. Chem. Lett. 1 (2010) 2193–2203, https://doi.org/10.1021/jz1005384.
[4] P.G. Bruce, S.A. Freunberger, L.J. Hardwick, J.M. Tarascon, LigO2 and LigS batteries with high energy storage, Nat. Mater. 11 (2012) 19–29, https://doi.org/10.1038/nmat3191.
[5] H. Yadegari, Q. Sun, X. Sun, Sodium-oxygen batteries: a comparative review from chemical and electrochemical fundamentals to future perspective, Adv. Mater. 28 (2016) 7065–7093, https://doi.org/10.1002/adma.201504373.
[6] B.D. McCloskey, A. Speidel, R. Scheffler, D.C. Miller, V. Viswanathan, J.S. Hummelshøj, J.K. Nørskov, A.C. Luntz, Twin problems of interfacial carbonate formation in nonaqueous Li–O 2 batteries, J. Phys. Chem. Lett. 3 (2012) 997–1001, https://doi.org/10.1021/jz300243r.
[7] B.D. McCloskey, A. Valery, A.C. Luntz, S.R. Gowda, G.M. Wallraff, J.M. Garcia, T. Mori, L.E. Krupp, Combining accurate O 2 and Li 2 O 2 assays to separate discharge and charge stability limitations in nonaqueous Li–O 2 batteries, J. Phys. Chem. Lett. 4 (2013) 2989–2993, https://doi.org/10.1021/jz401659f.
[8] M.M. Ottakam Thotiyl, S.A. Freunberger, Z. Peng, P.G. Bruce, The carbon electrode in nonaqueous Li–O 2 cells, J. Am. Chem. Soc. 135 (2013) 494–500, https://doi.org/10.1021/ja310258x.
[9] Z. Peng, S.A. Freunberger, L.J. Hardwick, Y. Chen, V. Giordani, F. Bardé, P. Novák, D. Graham, J.-M. Tarascon, P.G. Bruce, Oxygen reactions in a non-aqueous Li+ electrolyte, Angew. Chem. Int. Ed. 50 (2011) 6351–6355, https://doi.org/10.1002/anie.201100879.
[10] N.E. Benti, Y.S. Mekonnen, R. Christensen, G.A. Tiruye, J.M. Garcia-Lastra, T. Vegge, The effect of co2 contamination in rechargeable non-aqueous sodium-air batteries, J. Chem. Phys. 152 (2020), https://doi.org/10.1063/1.5141931.
[11] S.K. Das, S. Xu, L.A. Archer, Carbon dioxide assist for non-aqueous sodium-oxygen batteries, Electrochem. Commun. 27 (2013) 59–62, https://doi.org/10.1016/j.elecom.2012.10.036.
[12] W. Liu, Q. Sun, Y. Yang, J.-Y. Xie, Z.-W. Fu, An enhanced electrochemical performance of a sodium–air battery with graphene nanosheets as air electrode catalysts, Chem. Commun. 49 (2013) 1951, https://doi.org/10.1039/c3cc00085k.
[13] Y. Li, H. Yadegari, X. Li, M.N. Banis, R. Li, X. Sun, Superior catalytic activity of nitrogen-doped graphene cathodes for high energy capacity sodium–air batteries, Chem. Commun. 49 (2013) 11731, https://doi.org/10.1039/c3cc46606j.
[14] Z. Jian, Y. Chen, F. Li, T. Zhang, C. Liu, H. Zhou, High capacity Na–O2 batteries with carbon nanotube paper as binder-free air cathode, J. Power Sources 251 (2014) 466–469, https://doi.org/10.1016/j.jpowsour.2013.11.091.
[15] X. Bi, R. Wang, Y. Yuan, D. Zhang, T. Zhang, L. Ma, T. Wu, R. Shahbazian-Yassar, K. Amine, J. Lu, From sodium–oxygen to sodium–air battery: enabled by sodium peroxide dihydrate, Nano Lett. (2020), https://doi.org/10.1021/acs.nanolett.0c01670.
[16] X. Hu, P.H. Joo, E. Matios, C. Wang, J. Luo, K. Yang, W. Li, Designing an all-solid-state sodium-carbon dioxide battery enabled by nitrogen-doped nanocarbon, Nano Lett. 20 (2020) 3620–3626, https://doi.org/10.1021/acs.nanolett.0c00564.

[17] S. Xu, S. Lau, L.A. Archer, CO2 and ambient air in metal-oxygen batteries: steps towards reality, Inorg. Chem. Front. 2 (2015) 1070–1079, https://doi.org/10.1039/c5qi00169b.
[18] S. Xu, Y. Lu, H. Wang, H.D. Abruña, L.A. Archer, A rechargeable Na-CO2/O2 battery enabled by stable nanoparticle hybrid electrolytes, J. Mater. Chem. A. 2 (2014) 17723–17729, https://doi.org/10.1039/c4ta04130e.
[19] L. Zhang, Y. Tang, Q. Liu, T. Yang, C. Du, P. Jia, Z. Wang, Y. Tang, Y. Li, T. Shen, J. Huang, Probing the charging and discharging behavior of K-CO2 nanobatteries in an aberration corrected environmental transmission electron microscope, Nano Energy 53 (2018) 544–549, https://doi.org/10.1016/j.nanoen.2018.09.011.
[20] Y. Zhu, C. Li, Q. Wang, J. Wang, L. Chen, M. Gu, Fast lithiation of NiO investigated by in situ transmission electron microscopy, Appl. Phys. Lett. 115 (2019) 143902, https://doi.org/10.1063/1.5113871.
[21] Q. Liu, T. Yang, C. Du, Y. Tang, Y. Sun, P. Jia, J. Chen, H. Ye, T. Shen, Q. Peng, L. Zhang, J. Huang, In situ imaging the oxygen reduction reactions of solid state Na-O 2 batteries with CuO nanowires as the air cathode, Nano Lett. 18 (2018) 3723–3730, https://doi.org/10.1021/acs.nanolett.8b00894.
[22] L. Luo, B. Liu, S. Song, W. Xu, J. Zhang, C. Wang, Revealing the reaction mechanisms of Li – O2 batteries using environmental transmission electron mi .... Revealing the reaction mechanisms of Li – O 2 batteries using environmental transmission electron microscopy, Nat. Nanotechnol. 12 (2017) 535–540, https://doi.org/10.1038/nnano.2017.27.
[23] Y. Zhu, F. Yang, M. Guo, L. Chen, M. Gu, Real-time imaging of the electrochemical process in Na-O2Nanobatteries using Pt@CNT and Pt0.8Ir0.2@CNT air cathodes, ACS Nano 13 (2019) 14399–14407, https://doi.org/10.1021/acsnano.9b07961.
[24] Q. Liu, L. Geng, T. Yang, Y. Tang, P. Jia, Y. Li, H. Li, T. Shen, L. Zhang, J. Huang, In-situ imaging electrocatalysis in a Na-O2 battery with Au-coated MnO2 nanowires air cathode, Energy Storage Mater (2018), https://doi.org/10.1016/j.ensm.2018.08.026.
[25] Z. Liqiang, T. Yongfu, L.I.U. Qiunan, S.U.N. Haiming, Y. Tingting, H. Jianyu, Review of in Situ Transmission Electron Microscopy Studies of Battery Materials, 2019, p. 8, https://doi.org/10.12028/j.issn.2095-4239.2019.0117.
[26] X. Hu, Z. Li, Y. Zhao, J. Sun, Q. Zhao, J. Wang, Z. Tao, J. Chen, Quasi–solid state rechargeable Na-CO2 batteries with reduced graphene oxide Na anodes, Sci. Adv. 3 (2017) 1–8, https://doi.org/10.1126/sciadv.1602396.
[27] S.J. Hwang, S.J. Yoo, T.Y. Jeon, K.S. Lee, T.H. Lim, Y.E. Sung, S.K. Kim, Facile synthesis of highly active and stable Pt-Ir/C electrocatalysts for oxygen reduction and liquid fuel oxidation reaction, Chem. Commun. 46 (2010) 8401–8403, https://doi.org/10.1039/c0cc03125a.